Fabrication of High-Performance Ultrathin In_2O_3 Film Field-Effect Transistors and Biosensors Using Chemical Lift-Off Lithography

Jaemyung Kim,[†,‡,#] You Seung Rim,[†,§,#] Huajun Chen,[†,§] Huan H. Cao,[†,‡] Nako Nakatsuka,[†,‡] Hannah L. Hinton,[†,‡] Chuanzhen Zhao,[†,‡,⊥] Anne M. Andrews,[*,†,‡,∥] Yang Yang,[*,†,§] and Paul S. Weiss[*,†,‡,§]

[†]California NanoSystems Institute, University of California, Los Angeles, Los Angeles, California 90095, United States, [‡]Department of Chemistry and Biochemistry, University of California, Los Angeles, Los Angeles, California 90095, United States, [§]Department of Materials Science and Engineering, University of California, Los Angeles, Los Angeles, California 90095, United States, [⊥]Department of Materials Science and Engineering, Beijing Institute of Technology, Beijing 100081, China, and [∥]Department of Psychiatry and Semel Institute for Neuroscience and Human Behavior, University of California, Los Angeles, Los Angeles, California 90095, United States. [#]J. K. and Y. S. R. contributed equally to this work.

ABSTRACT We demonstrate straightforward fabrication of highly sensitive biosensor arrays based on field-effect transistors, using an efficient high-throughput, large-area patterning process. Chemical lift-off lithography is used to construct field-effect transistor arrays with high spatial precision suitable for the fabrication of both micrometer- and nanometer-scale devices. Sol–gel processing is used to deposit ultrathin (~4 nm) In_2O_3 films as semiconducting channel layers. The aqueous sol–gel process produces uniform In_2O_3 coatings with thicknesses of a few nanometers over large areas through simple spin-coating, and only low-temperature thermal annealing of the coatings is required. The ultrathin In_2O_3 enables construction of highly sensitive and selective biosensors through immobilization of specific aptamers to the channel surface; the ability to detect subnanomolar concentrations of dopamine is demonstrated.

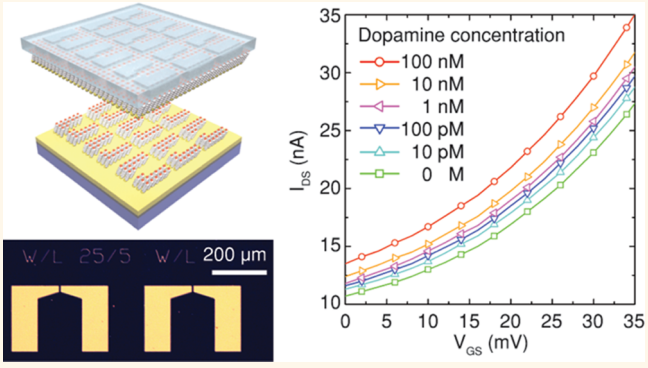

KEYWORDS: biosensor · field-effect transistor · chemical lift-off lithography · metal-oxide semiconductor · sol–gel chemistry · aptamer · neurotransmitter · dopamine · nanotechnology · nanofabrication · sensor

Field-effect transistors (FETs) have key advantages over optical or electrochemical platforms for biosensing applications, including low detection limits, real-time and label-free detection, and simple integration with standard semiconductor-device processing.[1−4] Biosensors based on FETs are typically constructed by immobilizing specific receptors on the surfaces of semiconducting channels. Upon specific interactions with target biomolecules, these receptors electrostatically gate the underlying channels and produce electronic signals such as changes in channel conductance and/or drain current. As the electronic signals of FET-based biosensors arise from the surface binding events between receptors and analytes, the sensitivity of devices is enhanced as the surface-to-volume ratio of the semiconducting channels increases. Therefore, nanomaterials with reduced dimensionalities and large surface areas are advantageous for the design of highly sensitive biosensors.

Notably, one-dimensional (1D) nanomaterials such as Si nanowires (SiNWs)[5−10] or carbon nanotubes (CNTs)[11−17] have been employed as the channel components of FET-based biosensors and shown to be highly effective in detecting biomolecules including proteins,[5,8,9,12−15] DNAs,[6,17] viruses,[18] and neurotransmitters.[7,10,19] More recently, two-dimensional (2D) nanomaterials such as graphene[20−24] and MoS_2[25,26] have attracted attention for biosensing applications as they are composed of surfaces

* Address correspondence to aandrews@mednet.ucla.edu, yangy@ucla.edu, psw@cnsi.ucla.edu.

Received for review February 23, 2015 and accepted March 23, 2015.

Published online March 23, 2015
10.1021/acsnano.5b01211

only and can thus provide remarkably large surface-to-volume ratios and high sensitivity.

One major challenge of using nanomaterials for FET-based biosensing applications is the complexity of the processes involved in their synthesis and integration into device platforms. For instance, both SiNWs and CNTs are typically synthesized by chemical vapor deposition (CVD),[27−30] which requires precise control of the growth parameters to produce high-quality 1D nanomaterials suitable for FETs. In the case of CNTs, the CVD process usually produces a mixture of nanotubes with varying electrical properties, and additional purification steps are needed to separate from the mixture the metallic CNTs that are not compatible with FET channel materials.[31−33] For large-scale applications of 2D nanostructures, both graphene[34−36] and MoS_2[37,38] are typically grown by CVD as well. After growth, transfer steps are required that can leave undesirable polymer residue on the surface that degrades device characteristics and/or the surface immobilization of receptors.[39−42]

Once nanomaterials are synthesized and placed on the desired substrates, lithography techniques are used to define device areas and to complete FET fabrication. Although conventional nanofabrication techniques such as photolithography or electron-beam lithography are effective in producing suitable electrode patterns for FET devices, they require the use of specialized equipment in clean, well-controlled environments. As such, there is a trade-off between spatial precision, cost, and throughput, limiting the scalability of high spatial precision patterning.

Here, we find that ultrathin (∼4 nm), amorphous metal-oxide semiconductor films produced *via* simple sol−gel chemistry are effective for the fabrication of highly sensitive FET-based biosensors. Oxide semiconductor thin films were formed over large areas through a simple spin-coating process. This fabrication step was followed by functionalization with biologically receptive moieties through oxide surface chemistry attachment. To define the electrode patterns and to construct the devices, we employed chemical lift-off lithography (CLL)[43] using self-assembled monolayers (SAMs) of alkanethiols on Au as soft masks. Through covalent interactions formed at the interfaces between hydroxyl-terminated alkanethiol SAMs and "activated" polydimethylsiloxane (PDMS) stamps, thiol molecules were selectively removed from predefined areas, exposing the underlying bare Au surfaces for subsequent wet-etching.

Chemical lift-off lithography provides an efficient tool for high-throughput prototyping of FET devices over large areas without the use of sophisticated instruments, producing device features with high spatial precision suitable for the fabrication of micrometer- and submicrometer-scale devices. By combining ultrathin oxide semiconductor layers with CLL, we demonstrate simple and straightforward fabrication of highly sensitive biosensors toward the detection of the small-molecule neurotransmitter dopamine down to physiological subnanomolar concentrations.

RESULTS AND DISCUSSION

We employed In_2O_3 as the channel material because its nanostructure has been shown to function effectively in biosensing platforms.[14,44−46] Moreover, thin films of In_2O_3 can be formed *via* simple aqueous sol−gel chemistry, resulting in few organic contaminants and enabling low-temperature processing.[47] We dissolved varying amounts of an indium precursor, indium(III) nitrate hydrate (99.999%), in water and spin-coated the solutions onto heavily doped Si substrates covered with 100 nm-thick, thermally grown SiO_2 dielectric layers. The substrates were then annealed at above 200 °C for 1 h to solidify the films.

As the indium precursor concentrations were increased, the color of the coated substrates changed from blue to light blue suggesting that the thicknesses of the deposited thin films increased. For the films prepared from solutions with low precursor concentrations (≤0.1 M), the color change was barely noticeable. When examined under an optical microscope, however, we found that solutions containing less than 0.1 M of indium precursor produced large pinholes in the resulting thin films (left panel, Figure 1a), which can cause discontinuous electrical conduction and are thus not suitable for thin-film devices. We determined that an indium precursor concentration of 0.1 M was the lower limit for spin-coating of uniform In_2O_3 films over large areas without pinholes (right panel, Figure 1a). Figure 1b and c show atomic force microscope (AFM) images of the resulting thin films. Even though the apparent thicknesses of these films were only ∼4 nm (Figure 1b), they showed high uniformity over large areas (30 μm × 30 μm in Figure 1c), and the root-mean-square roughness was calculated to be 0.4 nm.

We further examined these In_2O_3 films using non-destructive X-ray metrology. Figure 1d shows an X-ray diffraction (XRD) pattern of an In_2O_3 thin film prepared on a glass slide. Even after thermal annealing of the spin-coated film, no characteristic peak of In_2O_3 was observed, suggesting that the film was largely amorphous (a broad shoulder at around $2\theta \approx 25°$ corresponds to the background signal from the glass substrate). The thickness, mass density, and interface roughness of In_2O_3 films deposited on SiO_2/Si substrates were extracted by fitting X-ray reflectivity (XRR) curves to a standard model (Figure 1e). Film thicknesses were determined to be ∼3.8 nm, which agrees well with the apparent thickness measured by AFM (Figure 1b). The mass density of the films was estimated to be 5.90 g cm^{-3}, which is equivalent to 82.2% of the theoretical value of structurally perfect In_2O_3 crystals (7.18 g cm^{-3}). The roughness of the interface

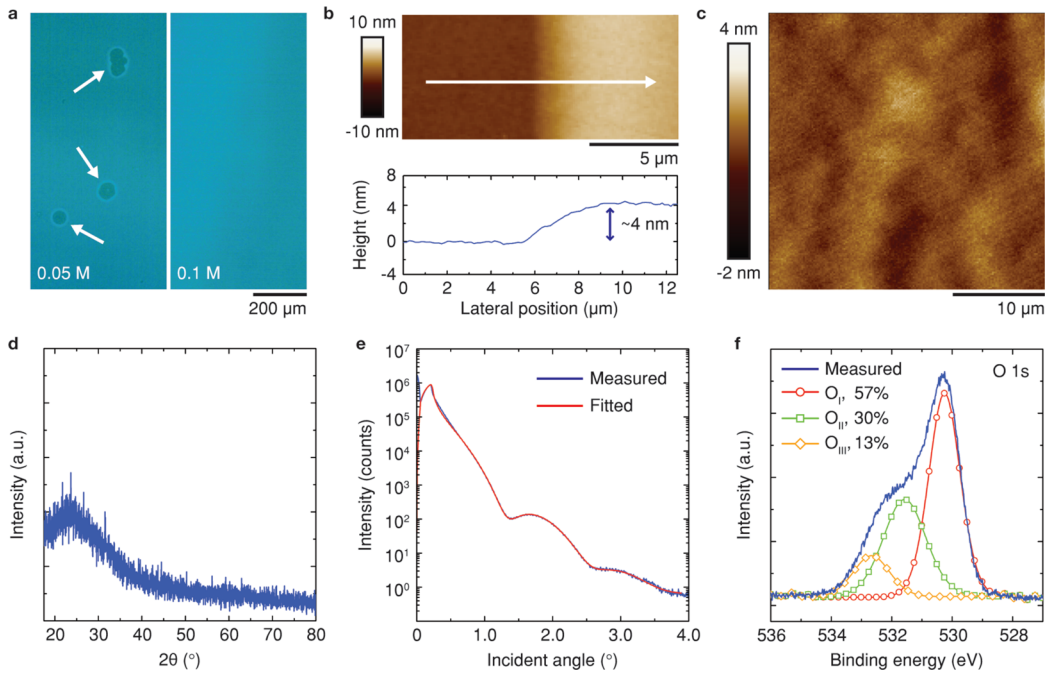

Figure 1. Sol–gel-processed In_2O_3 ultrathin films. Simple spin-coating of indium precursor solutions followed by thermal annealing enabled uncomplicated deposition of In_2O_3 layers with thicknesses measuring a few nanometers. (a) While a precursor solution containing 0.05 M of indium(III) nitrate produced a thin film with large pinholes (left, indicated by white arrows), a 0.1 M precursor solution produced a uniform thin film over large areas. (b, c) Atomic force microscope images of In_2O_3 thin film produced from a 0.1 M precursor solution; the sol–gel process produced a uniform film over large areas, with (b) an apparent thickness of 4 nm and (c) a root-mean-square roughness of 0.4 nm. (d) No characteristic peaks were observed in the X-ray diffraction pattern, suggesting the amorphous nature of the thin film. (e) The thickness, mass density, and interface roughness of the sol–gel processed In_2O_3 film were estimated to be 3.8 nm, 5.90 g cm^{-3}, and 0.4 nm, respectively, by fitting (red line) the X-ray reflectivity measurements (blue line) to a standard model. (f) The X-ray photoelectron O 1s spectrum of the ultrathin In_2O_3 layer shows that most of the peak can be assigned to O in the oxide lattice (O_I: O in oxide lattice without vacancies, O_{II}: O in oxide lattice with vacancies), while only 13% of O can be assigned to unreacted metal hydroxide species (O_{III}).

between In_2O_3 and SiO_2 was calculated to be ~0.4 nm. In general, the interface roughness is indicative of the interface trap density, which has direct effects on the electron-transport properties of FET devices.[48] With an interface roughness below 0.5 nm, the In_2O_3 films deposited on the SiO_2 dielectric layers are expected to show good switching behavior, as demonstrated in subsequent experiments. Figure 1f shows the O 1s spectrum of the annealed In_2O_3 films obtained by X-ray photoelectron spectroscopy (XPS). The spectrum was fit with and deconvoluted into three distinct peaks at 530.4, 531.5, and 532.6 eV, which correspond to O in the oxide lattice without vacancies (O_I), O in the oxide lattice with vacancies (O_{II}), and metal hydroxides (O_{III}), respectively.[47] We found that most of the O atoms reside in the oxide lattice while only 13% of O was assigned to unreacted metal hydroxide species, which is comparable to In_2O_3 films produced *via* organic-solvent-based approaches and annealed at high temperature.[47] On the basis of the XRD, XRR, and XPS measurements, we conclude that the aqueous-medium-based sol–gel process can produce, at relatively low temperatures, high-density amorphous In_2O_3 ultrathin films that are suitable for electronic applications.

To construct FET devices using the sol–gel-processed In_2O_3 films, we employed CLL as a high-throughput, large-scale tool to pattern Au source and drain contacts on SiO_2/Si substrates.[43] Figure 2a shows a schematic diagram depicting the CLL process. First, PDMS stamps with predesigned negative images of source-drain patterns were activated by oxygen plasma treatment and brought into conformal contact with hydroxyl-terminated alkanethiol SAMs, 11-mercapto-1-undecanol, deposited on Au surfaces (step 1). When the PDMS stamps were removed from the Au surfaces after 1 h of contact, thiol molecules in direct contact with the reactive PDMS surfaces were selectively removed owing to condensation reactions between the hydroxyl groups of the PDMS surfaces and the SAMs (step 2). The remaining SAMs on the Au surfaces acted as soft masks against subsequent chemical reactions, where the exposed bare Au surfaces and underlying Ti adhesion layers were selectively removed by wet etching (step 3). Remaining SAM molecules were then removed using oxygen plasma treatment (step 4), and ultrathin In_2O_3 layers were deposited on top of the electrode patterns *via* the sol–gel process (step 5). After thermal annealing, In_2O_3 films outside the channel areas were removed by 1 M HCl using photolithography-patterned masks (step 6).

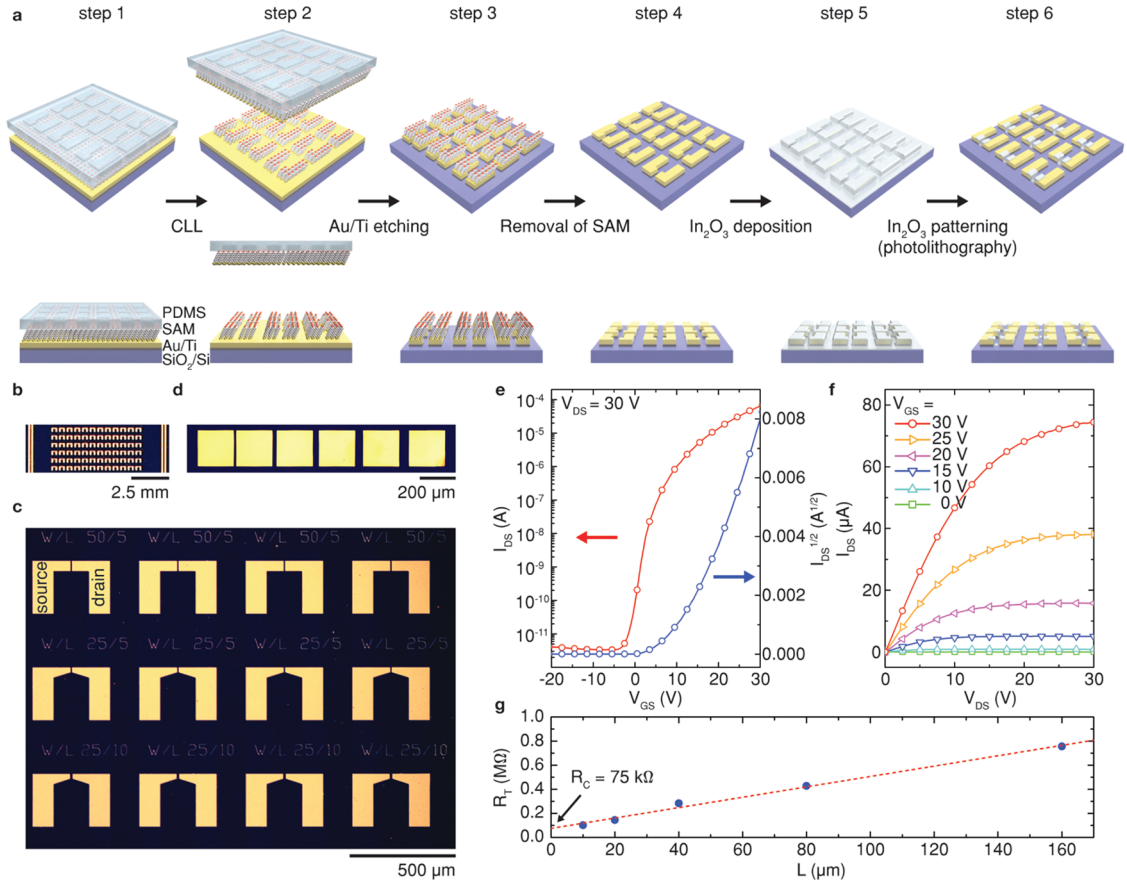

Figure 2. Field-effect transistor (FET) fabrication using chemical lift-off lithography (CLL). (a) Schematic illustration of FET fabrication steps using CLL. First, polydimethylsiloxane (PDMS) stamps with arrays of source and drain patterns were activated by oxygen plasma and brought into conformal contact with Au surfaces covered with self-assembled monolayers (SAMs) of hydroxyl-terminated alkanethiols (step 1). Through a condensation reaction between the hydroxyl groups of the PDMS surfaces and the SAMs, alkanethiol molecules in direct contact with the PDMS surfaces were selectively removed (step 2), leaving molecular patterns that served as soft masks during the following wet-etching of Au and Ti (step 3). After the metals were etched from the unprotected areas, the SAMs were removed by oxygen plasma (step 4) and ultrathin In_2O_3 layers were deposited through a sol−gel process (step 5). After thermal annealing, In_2O_3 films outside the channel areas were removed by wet-etching using photolithography-patterned masks (step 6). (b) Photograph showing 72 FET device patterns produced by CLL on a 100 nm SiO_2 layer on a Si substrate. (c, d) Optical microscope images of the CLL-produced device patterns over large areas showing (c) well-defined source and drain electrodes with channel gaps measuring a few micrometers and (d) a transmission line measurement (TLM) pattern with varying channel lengths. (e) Transfer and (f) output characteristics of the ultrathin In_2O_3 film FETs constructed atop the CLL-produced device patterns; the FETs showed good device performance with *n*-type pinch-off behavior with μ_{sat} of 11.5 ± 1.3 $cm^2 V^{-1} s^{-1}$ and I_{ON}/I_{OFF} of ~10^7. (g) R_C between In_2O_3 and the Au electrodes was estimated to be ~75 kΩ using the TLM pattern shown in (d).

Chemical lift-off lithography employs a strategy that is the inverse of conventional microcontact printing[49] as it leaves soft molecular masks on metal surfaces by subtractively patterning preformed SAMs. Compared to microcontact printing, which relies on the transfer of molecular inks from PDMS stamps to metal surfaces, both lateral diffusion and gas-phase deposition of ink molecules are avoided in CLL.[50,51] Thus, CLL produces high spatial precision, high-fidelity molecular masks that can be used to pattern underlying metal substrates. Figure 2b shows a photograph of 72 pairs of FET source−drain electrodes patterned over an area of 0.25 cm^2 using CLL. An optical microscope image of the Au patterns (Figure 2c) shows that the source and drain electrodes were well-defined and separated by channel gaps measuring a few micrometers. While we typically incubated Au surfaces in thiol solutions overnight and left the PDMS stamps on the substrates for 1 h, we found that this process could be shortened significantly. The patterns obtained after 5 min of SAM deposition and a 5 min stamping process also showed clear definition, comparable to patterns produced with longer processing times for the same spatial precision (see Supporting Information, Figure S1). The PDMS stamps could be used multiple times after simple rinsing and reactivation, reproducing patterns with similar qualities. A series of electrodes with varying channel lengths was also patterned on the same substrate for in-depth FET analysis (Figure 2d). Scanning electron microscope (SEM) images of the channel regions are shown in Figure S2 (see Supporting Information).

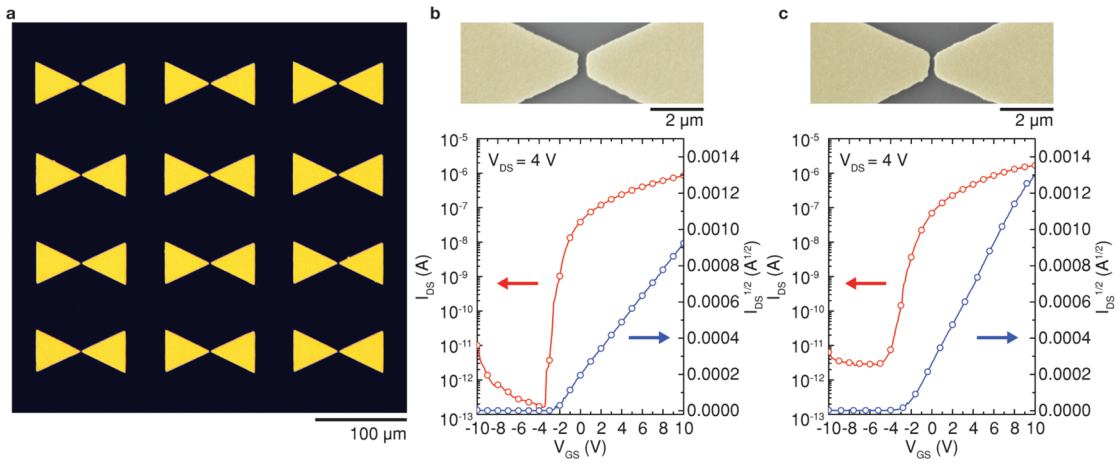

Figure 3. Fabrication of submicrometer-channel field-effect transistors (FETs) using chemical lift-off lithography (CLL). (a) Bow-tie device patterns with submicrometer channel lengths produced by CLL. (b, c) The top panels show scanning electron micrographs of the channel regions of the CLL-produced device patterns, with gap lengths measuring (b) 300 nm and (c) 150 nm. Transfer characteristics of the ultrathin (~4 nm) In_2O_3 film FETs fabricated atop the corresponding patterns are shown in the bottom panels. Compared to FETs with channel lengths measuring a few micrometers (Figure 2e), ultrathin In_2O_3 film FETs with submicrometer channel lengths can be operated at much lower V_{DS}. Reduction of the channel length to (c) 150 nm led to considerable degradation in device performance because of the short-channel effect. The values of μ_{sat}, I_{ON}/I_{OFF}, and SS of (b) 300 nm-channel FETs were calculated to be 0.6 ± 0.3 $cm^2 V^{-1} s^{-1}$, ~10^7, 0.3 ± 0.1 V dec^{-1}, respectively, while those for (c) 150 nm-channel FETs were calculated to be 0.4 ± 0.1 $cm^2 V^{-1} s^{-1}$, ~10^5, 0.6 ± 0.1 V dec^{-1}, respectively.

Figure 2e and f show representative transfer and output characteristics of bottom-gate bottom-contact (BGBC) In_2O_3 FET devices fabricated using CLL-patterned Au electrodes on SiO_2/Si substrates. In this structure, the channel width and length were 35 and 15 μm, respectively, and heavily doped Si substrates were used as gate electrodes. Different annealing conditions were tested and optimized device performance was obtained after the In_2O_3 thin films were annealed at 250 °C for 1 h (see Supporting Information, Figure S3). The optimized In_2O_3 FETs showed high field-effect mobilities (μ_{sat}) of 11.5 ± 1.3 $cm^2 V^{-1} s^{-1}$ (averaged over 50 devices) and on/off current ratios (I_{ON}/I_{OFF}) above 10^7. These performance characteristics are comparable to FETs with thicker In_2O_3 films fabricated *via* either organic-solvent-based sol−gel approaches[52−55] or sputtering[56,57] (see Supporting Information, Table S1).

The output characteristics of the FET devices (Figure 2f) showed *n*-type pinch-off behavior. The contact resistance (R_C) between In_2O_3 channels and Au electrodes was estimated by transmission-line measurements (TLMs; Figure 2g) using the pattern with varying channel lengths created by CLL (Figure 2d). Contact resistance was determined to be ~75 kΩ. We also fabricated bottom-gate top-contact (BGTC) In_2O_3 FETs by performing CLL on Au/Ti deposited on top of the semiconducting layers (see Supporting Information, Figure S4). The BGTC FETs showed better device performance compared to BGBC FETs, with μ_{sat} = 12.1 ± 3.5 $cm^2 V^{-1} s^{-1}$ and I_{ON}/I_{OFF} ~ 10^8. This improved performance was attributed to more favorable energy-level alignment at the interface between In_2O_3 channels and the Ti adhesion layers.[48] Detailed device parameters of BGBC ultrathin In_2O_3 film FETs processed under different annealing conditions and optimized BGTC devices are summarized in Table S2 (see Supporting Information).

Next, we scaled down the FET dimensions further and examined device performance of ultrathin In_2O_3 film FETs with submicrometer-scale channel lengths. Field-effect transistor miniaturization is integral for high-density device integration and enables low-voltage, low-power device operation. In a common laboratory setting, studies of FETs with submicrometer channel lengths are typically carried out with the aid of electron-beam lithography, which produces patterns with much finer features than photolithography. However, unlike photolithography, electron-beam lithography is a serial process and requires a considerable amount of time for patterning multiple devices over large areas. Chemical lift-off lithography enables facile prototyping of nanoscale devices as it enables parallel patterning of multiple devices over large areas with a spatial precision that can reach <20 nm.[43]

Figure 3a shows 12 Au source−drain electrode pairs with submicrometer channel lengths produced by CLL on a SiO_2/Si substrate. Bow-tie patterns with a large pad size were designed and used to ensure easy access by external electrodes. The top panels in Figure 3b and c show SEM images of the channel regions with gap lengths measuring 300 and 150 nm, respectively. High-magnification SEM images of the channel regions are shown in Figure S5 (see Supporting Information). Transfer characteristics of ultrathin In_2O_3 film FETs fabricated on the corresponding electrode patterns are shown in the bottom panels. Compared to devices with micrometer-scale channel lengths (Figure 2),

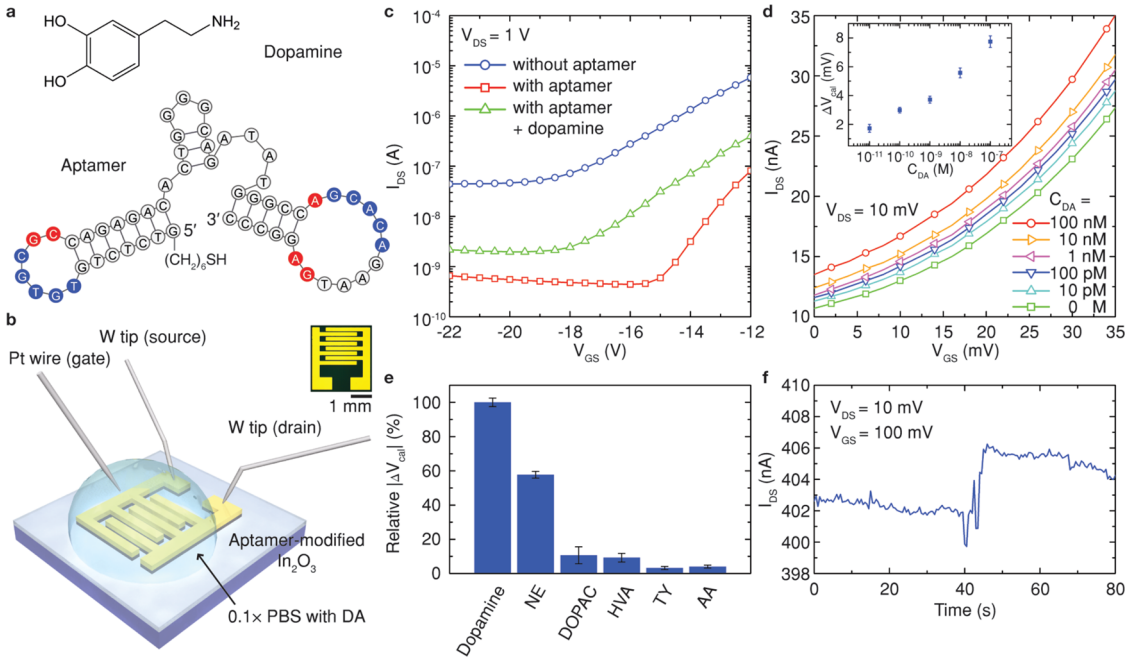

Figure 4. Aptamer−In_2O_3 biosensors for subnanomolar dopamine detection. The ultralow thickness of the sol−gel-processed In_2O_3 enabled the construction of highly sensitive dopamine biosensors by immobilizing (a) a DNA aptamer (bottom) that had specific binding with dopamine (top) on the oxide surface. The complementary and invariant bases for dopamine binding are indicated in blue and red, respectively. (b) Schematic diagram of the sensing setup; the aptamer−In_2O_3 biosensors operated with a liquid gate. The inset shows an interdigitated electrode pattern, fabricated using chemical lift-off lithography, used for the biosensors. (c) Dry state, Si back-gating measurements show that upon immobilization of the aptamer on the oxide surface, the transfer characteristics of ultrathin In_2O_3 film field-effect transistors (blue line) shifted downward (red line) and the turn-on voltage shifted toward positive values because of the electrostatic gating effect of negatively charged DNA on *n*-type In_2O_3. Positively charged dopamine binding to the aptamer partially recovered the drain current, with a shift of the turn-on voltage toward negative values (green line). (d) For the liquid-gate sensing experiments, the addition of dopamine to the liquid electrolyte also led to an increase in the drain current, and the linear working range of the aptamer−In_2O_3 biosensors was determined to be 10^{-11}−10^{-7} M (inset, ΔV_{cal}: calibrated response). (e) Calibrated responses of the aptamer−In_2O_3 biosensors upon exposure to 1 nM each of ascorbic acid (AA), tyramine (TY), homovanillic acid (HVA), 3,4-dihydroxyphenylacetic acid (DOPAC), and norepinephrine (NE). (f) Real-time sensing recording of 100 pM dopamine in 0.1× PBS, showing an increase in current upon exposure.

the nm-gap FETs can be operated at a significantly lower drain voltage (V_{DS}) of 4 V since the channel component of the series resistance scales down with decreasing channel lengths. Field-effect transistors with channel lengths of 300 nm (Figure 3b) showed steep switching behavior with a subthreshold swing (SS) of 0.3 ± 0.1 V dec^{-1}, which is significantly improved compared to the long-channel devices (Figure 2e; SS = 1.6 ± 0.1 V dec^{-1}). We hypothesize that this behavior is due to the reduced number of charge traps along the lateral direction and a decrease in sheet resistance as the channel length was decreased. The values of μ_{sat} and I_{ON}/I_{OFF} for these smaller FETs were 0.6 ± 0.3 $cm^2 V^{-1} s^{-1}$ and ~10^7, respectively. Further reduction of the channel length to 150 nm (Figure 3c) resulted in considerable degradation of device performance, with SS, μ_{sat}, and I_{ON}/I_{OFF} values of 0.6 ± 0.1 V dec^{-1}, 0.4 ± 0.1 $cm^2 V^{-1} s^{-1}$, and ~10^5, respectively. We attribute these adverse effects to drain-induced barrier lowering associated with short-channel FETs,[48] as evidenced by the negative shift in the turn-on voltage from −4 V (300 nm-channel FET) to −5 V (150 nm-channel FET). We expect that the performance of ultrathin In_2O_3 film FETs with sub-micrometer channel lengths can be further improved by employing advanced device architectures including lightly doped drains[48] or structures with double active layers.[58]

As charge transport through sol−gel-processed In_2O_3 thin films is confined within a few nanometers in the surface normal direction, electronic perturbation at the surface can significantly affect FET characteristics of the underlying metal oxide layer. Furthermore, various surface functionalization strategies available to metal oxides can be readily used to immobilize biospecific receptors on In_2O_3 thin films for selective detection of target molecules.[45] Therefore, ultrathin In_2O_3 layers can serve as platforms to construct highly sensitive and selective FET-based biosensors.

To test the ultrathin In_2O_3 FETs fabricated by CLL for biosensing applications, we investigated molecular recognition of the neurotransmitter dopamine using a previously identified dopamine aptamer (Figure 4a).[59−61] We investigated dopamine as a prototypical analyte because (i) it is a key neurotransmitter involved in brain reward and movement circuitries; dopaminergic neurons

are known to degenerate in Parkinson's disease,[62−65] and (ii) dopamine is a primary amine that carries a single positive charge at physiological pH, far less charge than that associated with biologically important macromolecular analytes such as proteins. Therefore, molecular recognition of dopamine at FET surfaces is expected to cause significantly less electronic perturbation than proteins. As such, dopamine is representative of an important class of biologically relevant small molecules that includes endogenous signaling molecules and drugs that are difficult to measure with simple devices.

To construct dopamine biosensors, we employed the BGTC structure that showed more favorable device characteristics (see Supporting Information, Table S2). To obtain large active sensor areas and uniform current distribution, interdigitated source and drain electrodes were used for biosensors. We first deposited ultrathin In_2O_3 layers on SiO_2/Si substrates, followed by Au/Ti depositions using electron-beam evaporation. The Au/Ti films were then patterned into interdigitated source and drain electrodes using CLL (Figure 4b). Subsequently, the hydroxyl-terminated alkanethiol SAMs used for CLL were removed by brief exposure to oxygen plasma, and 1-dodecanethiol was self-assembled on the Au surfaces to protect the electrodes from ensuing receptor immobilization. A thiol-terminated tethered DNA aptamer that recognizes dopamine, $HS(CH_2)_6$-5′-GTC TCT GTG TGC GCC AGA GAC ACT GGG GCA GAT ATG GGC CAG CAC AGA ATG AGG CCC-3′ (Figure 4a),[59−61] was immobilized on In_2O_3 surfaces using (3-aminopropyl)trimethoxysilane and 3-maleimidobenzoic acid *N*-hydroxysuccinimide ester as linkers to complete the biosensor fabrication.[10] Organosilanes form SAMs on various metal oxide surfaces with in-plane cross-linked Si−O−Si networks promoting dense molecular packing.[66−70] As the size of DNA aptamers is on the order of a few nanometers, steric hindrance may prohibit effective ligand−receptor binding unless aptamers are well-separated.[10] Therefore, trimethoxy(propyl)silane was codeposited on In_2O_3 surfaces and used as a spacer to optimize the surface density of aptamers for effective biosensing (see the Experimental Methods section).

Figure 4b shows a schematic illustration of the electrical measurement setup used for dopamine-sensing experiments. 0.1× phosphate-buffered saline (PBS, pH 7.4) was used as a liquid gate to detect signals effectively without severe Debye screening (Debye length ∼2.3 nm). Gate bias (V_{GS}) was applied through a Pt wire. Specific amounts of dopamine in 0.1× PBS were injected into the electrolyte solution to modulate dopamine concentrations in the liquid environment. To study the effect of the aptamer attachment to the channel surface, we first used highly doped Si substrates and 100 nm-thick SiO_2 layers as a back gate and a dielectric layer, respectively, and examined the changes in FET characteristics in a dry state upon aptamer immobilization (Figure 4c). We found that the attachment of aptamers to the channel surfaces caused over an order of magnitude decreases in the drain currents and positive shifts in the turn-on voltages (from −19 to −15 V). We attributed these effects to electrostatic gating effects of negatively charged DNA on the channel surfaces that result in decreases in carrier concentration of the *n*-type In_2O_3 layer. Upon incubation of the device in a 1 mM solution of dopamine for 1 h, the drain current partially recovered and the turn-on voltage shifted back to −18 V.

In general, aptamers undergo significant conformational changes upon binding with ligands,[71−75] which should affect the conductance modulation of underlying channel layers substantially. Since aptamers carry much greater charge than small molecules such as dopamine, their conformational changes are typically expected to dominate surface charge densities and surface charge density changes, as compared to the electrostatic gating effects of analytes. However, a previous study suggests that the dopamine-specific aptamer used in this work undergoes insufficient structural reorganization for electronic beacon approaches upon ligand binding.[61] Further studies will be needed to determine the specific charge redistribution and charge-sensing mechanism of our dopamine aptamer-based sensors, which will be critical to generalizing chemical sensing with these arrays.

Figure 4d shows the transfer characteristics of liquid-gated aptamer−In_2O_3 biosensors measured at various dopamine concentrations (C_{DA}) in solution. As in the case of measurements in a dry state, using a back-gated FET (Figure 4c), exposure of the biosensors to dopamine in a liquid-gate setup resulted in increased drain current. As C_{DA} was increased from 10 pM to 100 nM, the transfer characteristics of the device continuously shifted upward. No significant redox behavior of dopamine was observed in our device operating range (see Supporting Information, Figure S6), and the leakage current through the 0.1× PBS electrolyte was confirmed to be negligible (see Supporting Information, Figure S7). While further increases of C_{DA} to 1 μM or more resulted in continued upshift of the drain current, we found that nonspecific binding of dopamine to the channel surface became significant, and the drain current increased even without aptamer functionalization on the channel surface in this concentration range (see Supporting Information, Figure S8). To reduce device-to-device variations in sensor response, the change in drain current was converted to a change in gate voltage (calibrated response, ΔV_{cal}),[46] and the linear working range of the aptamer−In_2O_3 biosensor was determined to be 10^{-11}−10^{-7} M, as shown in the inset of Figure 4d.

We also constructed devices using an aptamer with mutations at identified dopamine binding sites

(mut-DA-aptamer, HS(CH_2)$_6$-5′-GTC TCT GTG TGC **TT**C AGA GAC ACT GGG GCA GAT ATG GGC C**T**G CAC AGA AT**T** **T**GG CCC-3′, mutated bases are highlighted in bold), as well as DNA with a random base sequence (scrambled-DNA, HS(CH_2)$_6$-5′-CAT AAA TAC TAG GAT GTG CAT ACT TAG ACT GGA GAT TGT ATC CCT ACA CAC ACC CTA-3′). Upon exposure of both devices to 10 nM dopamine in 0.1× PBS, we measured a ΔV_{cal} of less than 15% of the responses measured at devices constructed using the correct aptamer sequence (see Supporting Information, Figure S9). These results strongly suggest that sensor responses are based on specific interactions between dopamine and its cognate aptamer.

To test the selectivity of the aptamer−In_2O_3 biosensors, we exposed devices to 1 nM solutions of other similarly structured small molecules found in the brain extracellular environment.[76] Ascorbic acid (AA), tyramine (TY), homovanillic acid (HVA), 3,4-dihydroxyphenylacetic acid (DOPAC), and norepinephrine (NE) were dissolved in 0.1× PBS. Calibrated responses were then compared to responses to dopamine (Figure 4e). Although NE caused significant ΔV_{cal} that reached 58 ± 2% of the response to dopamine, all other tested biomolecules were associated with relative responses that were below 10% of the dopamine response. Cross reactivity of this aptamer with norepinephrine has been previously observed and reported.[10,61,77] We note that dopamine, NE, and TY caused increases in the drain current while AA, HVA, and DOPAC caused decreases, as the former group of molecules carry positive charges at physiological pH while the latter carry negative charges.

Finally, we performed real-time detection of dopamine in 0.1× PBS. The drain current of the aptamer−In_2O_3 device was continuously monitored at V_{DS} = 10 mV and V_{GS} = 100 mV while dopamine was introduced into the buffer solution. Figure 4f shows representative real-time sensing measurements obtained when the biosensor was exposed to a solution of 100 pM dopamine at t = 0. After a short delay associated with diffusion of dopamine to the channel surface, a sharp increase in drain current was observed. In comparison, the addition of buffer solution devoid of dopamine did not yield measurable changes in the drain current (data not shown).

CONCLUSIONS

A high-throughput and high spatial precision soft-lithography technique, CLL, was employed to produce device patterns with both micrometer- and submicrometer-scale feature sizes over large areas. This patterning method can be integrated with other processes to produce electronic device and biosensor arrays. Here, we have demonstrated that ultrathin In_2O_3 layers, produced by simple aqueous sol−gel processing, can be used as semiconducting active layers to construct high-performance FETs and biosensors. The as-fabricated In_2O_3 FETs showed effective device performance with μ_{sat} exceeding 10 $cm^2 V^{-1} s^{-1}$. The ultrathin In_2O_3 layers enabled construction of highly sensitive and selective aptamer-based biosensors capable of detecting subnanomolar concentrations of dopamine. The latter are more than sufficient to detect dopamine in the physiological range of basal extracellular brain levels.[78] Given this straightforward and effective device-fabrication strategy, we anticipate that CLL-patterned, sol−gel-processed metal-oxide FETs will enable platforms for the construction of both biological and nonbiological sensors that can detect subtle yet important chemical perturbations at interfaces.

EXPERIMENTAL METHODS

Materials. The DNA aptamer for dopamine was synthesized by Integrated DNA Technologies, Inc. (Coralville, IA). SYLGARD 184 from Dow Corning Corporation was used to make PDMS stamps throughout the work. All other chemicals were purchased from Sigma-Aldrich and used as received. Water was deionized before use (18.2 MΩ cm) using a Milli-Q system (Millipore, Billerica, MA).

Chemical Lift-off Lithography. Thin Au films (typically ~50 nm) were deposited on target substrates by electron-beam evaporation (CHA Industries, Fremont, CA) with Ti adhesion layers (5 nm). To deposit SAMs on Au surfaces, the substrates were immersed in 1 mM ethanolic solutions of 11-mercapto-1-undecanol and incubated overnight unless described otherwise. The PDMS stamps with defined patterns were prepared over masters fabricated by standard photolithography or electron-beam lithography. The stamps were exposed to oxygen plasma (Harrick Plasma, Ithaca, NY) at a power of 18 W and an oxygen pressure of 10 psi for 40 s to yield fully hydrophilic reactive surfaces, and brought into conformal contact with the SAM-modified Au surfaces. After 1 h, unless described otherwise, the stamps were carefully removed from the substrates, and an aqueous solution of 20 mM iron nitrate and 30 mM thiourea was applied to the substrates to etch Au films selectively from the area where the SAM was removed. Ti was removed from the exposed area using a 1:2 (v/v) solution of ammonium hydroxide and hydrogen peroxide. The substrates were rinsed with deionized water and dried under N_2 before use.

Fabrication of Field-Effect Transistors and Biosensors. Chemical lift-off lithography was performed to pattern source and drain Au electrodes on a heavily doped silicon wafer covered with a 100 nm-thick thermally grown SiO_2 layer. Aqueous solutions of varying indium(III) nitrate hydrate (99.999%) concentrations were spin-coated onto the substrates at 3000 rpm for 30 s. The substrates were then prebaked at 100 °C for 5 min followed by thermal annealing at 250 °C for 1 h. For top-contact devices, In_2O_3 layers and Au thin films were deposited successively by spin-coating and electron-beam evaporation, respectively, and CLL was performed to pattern source and drain electrodes. To make biosensors, a DNA aptamer that selectively binds to dopamine was immobilized on In_2O_3 layers with a top-contact device configuration. Briefly, CLL was used to pattern interdigitated Au source and drain electrodes atop the In_2O_3 layer deposited on a SiO_2/Si substrate. The substrate was then briefly exposed to oxygen plasma to remove the hydroxyl-terminated

alkanethiols from the Au surface, followed by incubation in a 1 mM ethanolic solution of 1-dodecanethiol for 1 h. After thorough rinsing with ethanol, (3-aminopropyl)trimethoxysilane and trimethoxy(propyl)silane (1:9, v/v) were thermally evaporated to the In_2O_3 surface at 40 °C for 1 h, and the substrate was immersed in a 1 mM solution of 3-maleimidobenzoic acid *N*-hydroxysuccinimide ester dissolved in 1:9 (v/v) mixture of dimethyl sulfoxide and 1× PBS for 30 min. To anchor the DNA aptamer, the substrate was rinsed with deionized water, immersed in a 1 μM solution of thiolated DNA in 1× PBS for 1 h, rinsed again with deionized water and blown dried with N_2.

Characterization. Optical microscopy images were taken with Olympus BX51M. Atomic force microscopy imaging was performed on a Bruker Dimension Icon system under tapping mode. X-ray diffraction and XRR measurements were performed on a PANalytical X'Pert Pro system and a Bede D1 diffractometer, respectively. X-ray photoelectron spectra were collected on a Kratos Axis Ultra DLD system. Cyclic voltammetry was performed using a PAR EG&G 273A Potentiostat with a Ag/AgCl electrode, a platinum foil, and a platinum wire as a reference electrode, a counter electrode, and a working electrode, respectively. The measurement was performed in a 0.1× PBS at a voltage sweep rate of 50 mV s^{-1}. All electrical measurements were performed on a probe station equipped with an Agilent 4155C semiconductor analyzer. At least 10 devices were tested for each biosensing experiment, and the five best devices in terms of stable (*i.e.*, low drift) baseline currents were selected to obtain statistical data.

Conflict of Interest: The authors declare no competing financial interest.

Acknowledgment. We gratefully acknowledge the support of the Kavli Foundation for this work. Y. S. R., H. C., and Y. Y. acknowledge financial support from the National Science Foundation (ECCS-1202231; Program Director: Dr. Paul Werbos). H. H. C., N. N., and A. M. A. acknowledge support from the UCLA Weil Endowment Fund for Research. H. L. H. and C. Z. are grateful to the CARE SEM Summer Research Program and Cross-Disciplinary Scholars in Science and Technology (CSST) Program at UCLA, respectively, for financial support. We thank the Nano and Pico Characterization Lab and the Integrated Systems Nanofabrication Cleanroom at the California NanoSystems Institute, and the UCLA Molecular Instrumentation Center for the use of their facilities. J. K. and Y. S. R. conceived the study, conducted the experiments, and analyzed the data. H. C., H. H. C., N. N., H. L. H., and C. Z. provided assistance in data acquisition and designing experiments. A. M. A., Y. Y., and P. S. W. supervised the project and cowrote the manuscript with J. K. and Y. S. R.

Supporting Information Available: An optical micrograph of device patterns produced by CLL with shorter processing times, scanning electron microscope images of CLL-patterned devices, transfer characteristics of BGBC ultrathin In_2O_3 film FETs processed under different annealing conditions, a device performance chart of previously reported In_2O_3 field-effect transistors, transfer and output characteristics of optimized BGTC devices, a summary of detailed device performance parameters, a cyclic voltammogram of a Pt wire in 0.1× PBS, a leakage current measurement through the liquid electrolyte, and responses of In_2O_3 FETs to dopamine exposures with modified aptamer sequences and without aptamer immobilization. This material is available free of charge *via* the Internet at http://pubs.acs.org.

REFERENCES AND NOTES

1. Schoning, M. J.; Poghossian, A. Recent Advances in Biologically Sensitive Field-Effect Transistors (BioFETs). *Analyst* **2002**, *127*, 1137–1151.
2. Patolsky, F.; Lieber, C. M. Nanowire Nanosensors. *Mater. Today* **2005**, *8*, 20–28.
3. Allen, B. L.; Kichambare, P. D.; Star, A. Carbon Nanotube Field-Effect-Transistor-Based Biosensors. *Adv. Mater.* **2007**, *19*, 1439–1451.
4. Curreli, M.; Rui, Z.; Ishikawa, F. N.; Chang, H.-K.; Cote, R. J.; Chongwu, Z.; Thompson, M. E. Real-Time, Label-Free Detection of Biological Entities Using Nanowire-Based FETs. *IEEE Trans. Nanotechnol.* **2008**, *7*, 651–667.
5. Cui, Y.; Wei, Q.; Park, H.; Lieber, C. M. Nanowire Nanosensors for Highly Sensitive and Selective Detection of Biological and Chemical Species. *Science* **2001**, *293*, 1289–1292.
6. Hahm, J.-I.; Lieber, C. M. Direct Ultrasensitive Electrical Detection of DNA and DNA Sequence Variations Using Nanowire Nanosensors. *Nano Lett.* **2003**, *4*, 51–54.
7. Wang, W. U.; Chen, C.; Lin, K.-H.; Fang, Y.; Lieber, C. M. Label-Free Detection of Small-Molecule–Protein Interactions by Using Nanowire Nanosensors. *Proc. Natl. Acad. Sci. U. S. A.* **2005**, *102*, 3208–3212.
8. Zheng, G.; Patolsky, F.; Cui, Y.; Wang, W. U.; Lieber, C. M. Multiplexed Electrical Detection of Cancer Markers with Nanowire Sensor Arrays. *Nat. Biotechnol.* **2005**, *23*, 1294–1301.
9. Stern, E.; Klemic, J. F.; Routenberg, D. A.; Wyrembak, P. N.; Turner-Evans, D. B.; Hamilton, A. D.; LaVan, D. A.; Fahmy, T. M.; Reed, M. A. Label-Free Immunodetection with CMOS-Compatible Semiconducting Nanowires. *Nature* **2007**, *445*, 519–522.
10. Li, B.-R.; Hsieh, Y.-J.; Chen, Y.-X.; Chung, Y.-T.; Pan, C.-Y.; Chen, Y.-T. An Ultrasensitive Nanowire-Transistor Biosensor for Detecting Dopamine Release from Living PC12 Cells under Hypoxic Stimulation. *J. Am. Chem. Soc.* **2013**, *135*, 16034–16037.
11. Besteman, K.; Lee, J.-O.; Wiertz, F. G. M.; Heering, H. A.; Dekker, C. Enzyme-Coated Carbon Nanotubes as Single-Molecule Biosensors. *Nano Lett.* **2003**, *3*, 727–730.
12. Chen, R. J.; Bangsaruntip, S.; Drouvalakis, K. A.; Kam, N. W. S.; Shim, M.; Li, Y.; Kim, W.; Utz, P. J.; Dai, H. Noncovalent Functionalization of Carbon Nanotubes for Highly Specific Electronic Biosensors. *Proc. Natl. Acad. Sci. U. S. A.* **2003**, *100*, 4984–4989.
13. So, H.-M.; Won, K.; Kim, Y. H.; Kim, B.-K.; Ryu, B. H.; Na, P. S.; Kim, H.; Lee, J.-O. Single-Walled Carbon Nanotube Biosensors Using Aptamers as Molecular Recognition Elements. *J. Am. Chem. Soc.* **2005**, *127*, 11906–11907.
14. Tang, T.; Liu, X.; Li, C.; Lei, B.; Zhang, D.; Rouhanizadeh, M.; Hsiai, T.; Zhou, C. Complementary Response of In_2O_3 Nanowires and Carbon Nanotubes to Low-Density Lipoprotein Chemical Gating. *Appl. Phys. Lett.* **2005**, *86*, 103903.
15. Maehashi, K.; Katsura, T.; Kerman, K.; Takamura, Y.; Matsumoto, K.; Tamiya, E. Label-Free Protein Biosensor Based on Aptamer-Modified Carbon Nanotube Field-Effect Transistors. *Anal. Chem.* **2006**, *79*, 782–787.
16. Kim, S. N.; Rusling, J. F.; Papadimitrakopoulos, F. Carbon Nanotubes for Electronic and Electrochemical Detection of Biomolecules. *Adv. Mater.* **2007**, *19*, 3214–3228.
17. Martínez, M. T.; Tseng, Y.-C.; Ormategui, N.; Loinaz, I.; Eritja, R.; Bokor, J. Label-Free DNA Biosensors Based on Functionalized Carbon Nanotube Field Effect Transistors. *Nano Lett.* **2009**, *9*, 530–536.
18. Patolsky, F.; Zheng, G.; Hayden, O.; Lakadamyali, M.; Zhuang, X.; Lieber, C. M. Electrical Detection of Single Viruses. *Proc. Natl. Acad. Sci. U. S. A.* **2004**, *101*, 14017–14022.
19. Alivisatos, A. P.; Andrews, A. M.; Boyden, E. S.; Chun, M.; Church, G. M.; Deisseroth, K.; Donoghue, J. P.; Fraser, S. E.; Lippincott-Schwartz, J.; Looger, L. L.; *et al.* Nanotools for Neuroscience and Brain Activity Mapping. *ACS Nano* **2013**, *7*, 1850–1866.
20. Ohno, Y.; Maehashi, K.; Matsumoto, K. Label-Free Biosensors Based on Aptamer-Modified Graphene Field-Effect Transistors. *J. Am. Chem. Soc.* **2010**, *132*, 18012–18013.
21. Huang, Y.; Dong, X.; Shi, Y.; Li, C. M.; Li, L.-J.; Chen, P. Nanoelectronic Biosensors Based on CVD Grown Graphene. *Nanoscale* **2010**, *2*, 1485–1488.
22. Yang, W.; Ratinac, K. R.; Ringer, S. P.; Thordarson, P.; Gooding, J. J.; Braet, F. Carbon Nanomaterials in Biosensors: Should You Use Nanotubes or Graphene? *Angew. Chem., Int. Ed.* **2010**, *49*, 2114–2138.

23. Pumera, M. Graphene in Biosensing. *Mater. Today* **2011**, *14*, 308–315.
24. He, Q.; Sudibya, H. G.; Yin, Z.; Wu, S.; Li, H.; Boey, F.; Huang, W.; Chen, P.; Zhang, H. Centimeter-Long and Large-Scale Micropatterns of Reduced Graphene Oxide Films: Fabrication and Sensing Applications. *ACS Nano* **2010**, *4*, 3201–3208.
25. Sarkar, D.; Liu, W.; Xie, X.; Anselmo, A. C.; Mitragotri, S.; Banerjee, K. MoS_2 Field-Effect Transistor for Next-Generation Label-Free Biosensors. *ACS Nano* **2014**, *8*, 3992–4003.
26. Wang, L.; Wang, Y.; Wong, J. I.; Palacios, T.; Kong, J.; Yang, H. Y. Functionalized MoS_2 Nanosheet-Based Field-Effect Biosensor for Label-Free Sensitive Detection of Cancer Marker Proteins in Solution. *Small* **2014**, *10*, 1101–1105.
27. Morales, A. M.; Lieber, C. M. A Laser Ablation Method for the Synthesis of Crystalline Semiconductor Nanowires. *Science* **1998**, *279*, 208–211.
28. Hochbaum, A. I.; Fan, R.; He, R.; Yang, P. Controlled Growth of Si Nanowire Arrays for Device Integration. *Nano Lett.* **2005**, *5*, 457–460.
29. Fan, S.; Chapline, M. G.; Franklin, N. R.; Tombler, T. W.; Cassell, A. M.; Dai, H. Self-Oriented Regular Arrays of Carbon Nanotubes and Their Field Emission Properties. *Science* **1999**, *283*, 512–514.
30. Hata, K.; Futaba, D. N.; Mizuno, K.; Namai, T.; Yumura, M.; Iijima, S. Water-Assisted Highly Efficient Synthesis of Impurity-Free Single-Walled Carbon Nanotubes. *Science* **2004**, *306*, 1362–1364.
31. Hersam, M. C. Progress Towards Monodisperse Single-Walled Carbon Nanotubes. *Nat. Nanotechnol.* **2008**, *3*, 387–394.
32. Arnold, M. S.; Green, A. A.; Hulvat, J. F.; Stupp, S. I.; Hersam, M. C. Sorting Carbon Nanotubes by Electronic Structure Using Density Differentiation. *Nat. Nanotechnol.* **2006**, *1*, 60–65.
33. Zheng, M.; Jagota, A.; Strano, M. S.; Santos, A. P.; Barone, P.; Chou, S. G.; Diner, B. A.; Dresselhaus, M. S.; Mclean, R. S.; Onoa, G. B.; *et al.* Structure-Based Carbon Nanotube Sorting by Sequence-Dependent DNA Assembly. *Science* **2003**, *302*, 1545–1548.
34. Sun, Z.; Yan, Z.; Yao, J.; Beitler, E.; Zhu, Y.; Tour, J. M. Growth of Graphene from Solid Carbon Sources. *Nature* **2010**, *468*, 549–552.
35. Li, X.; Cai, W.; An, J.; Kim, S.; Nah, J.; Yang, D.; Piner, R.; Velamakanni, A.; Jung, I.; Tutuc, E.; *et al.* Large-Area Synthesis of High-Quality and Uniform Graphene Films on Copper Foils. *Science* **2009**, *324*, 1312–1314.
36. Bai, J.; Liao, L.; Zhou, H.; Cheng, R.; Liu, L.; Huang, Y.; Duan, X. Top-Gated Chemical Vapor Deposition Grown Graphene Transistors with Current Saturation. *Nano Lett.* **2011**, *11*, 2555–2559.
37. Lee, Y.-H.; Zhang, X.-Q.; Zhang, W.; Chang, M.-T.; Lin, C.-T.; Chang, K.-D.; Yu, Y.-C.; Wang, J. T.-W.; Chang, C.-S.; Li, L.-J.; *et al.* Synthesis of Large-Area MoS_2 Atomic Layers with Chemical Vapor Deposition. *Adv. Mater.* **2012**, *24*, 2320–2325.
38. Lee, Y.-H.; Yu, L.; Wang, H.; Fang, W.; Ling, X.; Shi, Y.; Lin, C.-T.; Huang, J.-K.; Chang, M.-T.; Chang, C.-S.; *et al.* Synthesis and Transfer of Single-Layer Transition Metal Disulfides on Diverse Surfaces. *Nano Lett.* **2013**, *13*, 1852–1857.
39. Li, X.; Zhu, Y.; Cai, W.; Borysiak, M.; Han, B.; Chen, D.; Piner, R. D.; Colombo, L.; Ruoff, R. S. Transfer of Large-Area Graphene Films for High-Performance Transparent Conductive Electrodes. *Nano Lett.* **2009**, *9*, 4359–4363.
40. Lee, Y.; Bae, S.; Jang, H.; Jang, S.; Zhu, S.-E.; Sim, S. H.; Song, Y. I.; Hong, B. H.; Ahn, J.-H. Wafer-Scale Synthesis and Transfer of Graphene Films. *Nano Lett.* **2010**, *10*, 490–493.
41. Lin, Y.-C.; Lu, C.-C.; Yeh, C.-H.; Jin, C.; Suenaga, K.; Chiu, P.-W. Graphene Annealing: How Clean Can It Be? *Nano Lett.* **2011**, *12*, 414–419.
42. Pirkle, A.; Chan, J.; Venugopal, A.; Hinojos, D.; Magnuson, C. W.; McDonnell, S.; Colombo, L.; Vogel, E. M.; Ruoff, R. S.; Wallace, R. M. The Effect of Chemical Residues on the Physical and Electrical Properties of Chemical Vapor Deposited Graphene Transferred to SiO_2. *Appl. Phys. Lett.* **2011**, *99*, 122108.
43. Liao, W.-S.; Cheunkar, S.; Cao, H. H.; Bednar, H. R.; Weiss, P. S.; Andrews, A. M. Subtractive Patterning *via* Chemical Lift-Off Lithography. *Science* **2012**, *337*, 1517–1521.
44. Ishikawa, F. N.; Chang, H.-K.; Curreli, M.; Liao, H.-I.; Olson, C. A.; Chen, P.-C.; Zhang, R.; Roberts, R. W.; Sun, R.; Cote, R. J.; *et al.* Label-Free, Electrical Detection of the SARS Virus N-Protein with Nanowire Biosensors Utilizing Antibody Mimics as Capture Probes. *ACS Nano* **2009**, *3*, 1219–1224.
45. Curreli, M.; Li, C.; Sun, Y.; Lei, B.; Gundersen, M. A.; Thompson, M. E.; Zhou, C. Selective Functionalization of In_2O_3 Nanowire Mat Devices for Biosensing Applications. *J. Am. Chem. Soc.* **2005**, *127*, 6922–6923.
46. Ishikawa, F. N.; Curreli, M.; Chang, H.-K.; Chen, P.-C.; Zhang, R.; Cote, R. J.; Thompson, M. E.; Zhou, C. A Calibration Method for Nanowire Biosensors to Suppress Device-to-Device Variation. *ACS Nano* **2009**, *3*, 3969–3976.
47. Hwang, Y. H.; Seo, J.-S.; Yun, J. M.; Park, H.; Yang, S.; Park, S.-H. K.; Bae, B.-S. An 'Aqueous Route' for the Fabrication of Low-Temperature-Processable Oxide Flexible Transparent Thin-Film Transistors on Plastic Substrates. *NPG Asia Mater.* **2013**, *5*, e45.
48. Sze, S. M.; Ng, K. K. *Physics of Semiconductor Devices*, 3rd ed.; Wiley-Interscience: Hoboken, NJ, 2007; pp 293−373.
49. Kumar, A.; Whitesides, G. M. Features of Gold Having Micrometer to Centimeter Dimensions Can Be Formed through a Combination of Stamping with an Elastomeric Stamp and an Alkanethiol "Ink" Followed by Chemical Etching. *Appl. Phys. Lett.* **1993**, *63*, 2002–2004.
50. Srinivasan, C.; Mullen, T. J.; Hohman, J. N.; Anderson, M. E.; Dameron, A. A.; Andrews, A. M.; Dickey, E. C.; Horn, M. W.; Weiss, P. S. Scanning Electron Microscopy of Nanoscale Chemical Patterns. *ACS Nano* **2007**, *1*, 191–201.
51. Braunschweig, A. B.; Huo, F.; Mirkin, C. A. Molecular Printing. *Nat. Chem.* **2009**, *1*, 353–358.
52. Kim, H. S.; Byrne, P. D.; Facchetti, A.; Marks, T. J. High Performance Solution-Processed Indium Oxide Thin-Film Transistors. *J. Am. Chem. Soc.* **2008**, *130*, 12580–12581.
53. Rim, Y. S.; Lim, H. S.; Kim, H. J. Low-Temperature Metal-Oxide Thin-Film Transistors Formed by Directly Photopatternable and Combustible Solution Synthesis. *ACS Appl. Mater. Interfaces* **2013**, *5*, 3565–3571.
54. Choi, C.-H.; Han, S.-Y.; Su, Y.-W.; Fang, Z.; Lin, L.-Y.; Cheng, C.-C.; Chang, C.-H. Fabrication of High-Performance, Low-Temperature Solution Processed Amorphous Indium Oxide Thin-Film Transistors Using a Volatile Nitrate Precursor. *J. Mater. Chem. C* **2015**, *3*, 854–860.
55. Kim, M.-G.; Kanatzidis, M. G.; Facchetti, A.; Marks, T. J. Low-Temperature Fabrication of High-Performance Metal Oxide Thin-Film Electronics *via* Combustion Processing. *Nat. Mater.* **2011**, *10*, 382–388.
56. Joo Hyon, N.; Seung Yoon, R.; Sung Jin, J.; Chang Su, K.; Sung-Woo, S.; Rack, P. D.; Dong-Joo, K.; Hong Koo, B. Indium Oxide Thin-Film Transistors Fabricated by RF Sputtering at Room Temperature. *IEEE Electron Device Lett.* **2010**, *31*, 567–569.
57. Jiao, Y.; Zhang, X.; Zhai, J.; Yu, X.; Ding, L.; Zhang, W. Bottom-Gate Amorphous In_2O_3 Thin Film Transistors Fabricated by Magnetron Sputtering. *Electron. Mater. Lett.* **2013**, *9*, 279–282.
58. Rim, Y. S.; Chen, H.; Kou, X.; Duan, H.-S.; Zhou, H.; Cai, M.; Kim, H. J.; Yang, Y. Boost Up Mobility of Solution-Processed Metal Oxide Thin-Film Transistors *via* Confining Structure on Electron Pathways. *Adv. Mater.* **2014**, *26*, 4273–4278.
59. Mannironi, C.; Di Nardo, A.; Fruscoloni, P.; Tocchini-Valentini, G. P. *In Vitro* Selection of Dopamine RNA Ligands. *Biochemistry* **1997**, *36*, 9726–9734.
60. Walsh, R.; DeRosa, M. C. Retention of Function in the DNA Homolog of the RNA Dopamine Aptamer. *Biochem. Biophys. Res. Commun.* **2009**, *388*, 732–735.
61. Farjami, E.; Campos, R.; Nielsen, J. S.; Gothelf, K. V.; Kjems, J.; Ferapontova, E. E. RNA Aptamer-Based Electrochemical Biosensor for Selective and Label-Free Analysis of Dopamine. *Anal. Chem.* **2012**, *85*, 121–128.
62. Giros, B.; Jaber, M.; Jones, S. R.; Wightman, R. M.; Caron, M. G. Hyperlocomotion and Indifference to Cocaine and

Amphetamine in Mice Lacking the Dopamine Transporter. *Nature* **1996**, *379*, 606–612.
63. Kim, J.-H.; Auerbach, J. M.; Rodriguez-Gomez, J. A.; Velasco, I.; Gavin, D.; Lumelsky, N.; Lee, S.-H.; Nguyen, J.; Sanchez-Pernaute, R.; Bankiewicz, K.; *et al.* Dopamine Neurons Derived from Embryonic Stem Cells Function in an Animal Model of Parkinson's Disease. *Nature* **2002**, *418*, 50–56.
64. Phillips, P. E. M.; Stuber, G. D.; Heien, M. L. A. V.; Wightman, R. M.; Carelli, R. M. Subsecond Dopamine Release Promotes Cocaine Seeking. *Nature* **2003**, *422*, 614–618.
65. Unger, E. L.; Eve, D. J.; Perez, X. A.; Reichenbach, D. K.; Xu, Y.; Lee, M. K.; Andrews, A. M. Locomotor Hyperactivity and Alterations in Dopamine Neurotransmission Are Associated with Overexpression of A53T Mutant Human α-Synuclein in Mice. *Neurobiol. Dis.* **2006**, *21*, 431–443.
66. Aswal, D. K.; Lenfant, S.; Guerin, D.; Yakhmi, J. V.; Vuillaume, D. Self Assembled Monolayers on Silicon for Molecular Electronics. *Anal. Chim. Acta* **2006**, *568*, 84–108.
67. Helmy, R.; Fadeev, A. Y. Self-Assembled Monolayers Supported on TiO_2: Comparison of $C_{18}H_{37}SiX_3$ (X = H, Cl, OCH_3), $C_{18}H_{37}Si(CH_3)_2Cl$, and $C_{18}H_{37}PO(OH)_2$. *Langmuir* **2002**, *18*, 8924–8928.
68. Kim, J. S.; Park, J. H.; Lee, J. H.; Jo, J.; Kim, D.-Y.; Cho, K. Control of the Electrode Work Function and Active Layer Morphology *via* Surface Modification of Indium Tin Oxide for High Efficiency Organic Photovoltaics. *Appl. Phys. Lett.* **2007**, *91*, 112111.
69. Chung, Y.; Verploegen, E.; Vailionis, A.; Sun, Y.; Nishi, Y.; Murmann, B.; Bao, Z. Controlling Electric Dipoles in Nano-dielectrics and Its Applications for Enabling Air-Stable N-Channel Organic Transistors. *Nano Lett.* **2011**, *11*, 1161–1165.
70. Song, C. K.; Luck, K. A.; Zhou, N.; Zeng, L.; Heitzer, H. M.; Manley, E. F.; Goldman, S.; Chen, L. X.; Ratner, M. A.; Bedzyk, M. J.; *et al.* "Supersaturated" Self-Assembled Charge-Selective Interfacial Layers for Organic Solar Cells. *J. Am. Chem. Soc.* **2014**, *136*, 17762–17773.
71. Baker, B. R.; Lai, R. Y.; Wood, M. S.; Doctor, E. H.; Heeger, A. J.; Plaxco, K. W. An Electronic, Aptamer-Based Small-Molecule Sensor for the Rapid, Label-Free Detection of Cocaine in Adulterated Samples and Biological Fluids. *J. Am. Chem. Soc.* **2006**, *128*, 3138–3139.
72. Ferapontova, E. E.; Olsen, E. M.; Gothelf, K. V. An RNA Aptamer-Based Electrochemical Biosensor for Detection of Theophylline in Serum. *J. Am. Chem. Soc.* **2008**, *130*, 4256–4258.
73. Fan, C.; Plaxco, K. W.; Heeger, A. J. Electrochemical Interrogation of Conformational Changes as a Reagentless Method for the Sequence-Specific Detection of DNA. *Proc. Natl. Acad. Sci. U. S. A.* **2003**, *100*, 9134–9137.
74. Zuo, X.; Song, S.; Zhang, J.; Pan, D.; Wang, L.; Fan, C. A Target-Responsive Electrochemical Aptamer Switch (TREAS) for Reagentless Detection of Nanomolar ATP. *J. Am. Chem. Soc.* **2007**, *129*, 1042–1043.
75. Farjami, E.; Clima, L.; Gothelf, K.; Ferapontova, E. E. "Off−On" Electrochemical Hairpin-DNA-Based Genosensor for Cancer Diagnostics. *Anal. Chem.* **2011**, *83*, 1594–1602.
76. Singh, Y. S.; Sawarynski, L. E.; Dabiri, P. D.; Choi, W. R.; Andrews, A. M. Head-to-Head Comparisons of Carbon Fiber Microelectrode Coatings for Sensitive and Selective Neurotransmitter Detection by Voltammetry. *Anal. Chem.* **2011**, *83*, 6658–6666.
77. Zheng, Y.; Wang, Y.; Yang, X. Aptamer-Based Colorimetric Biosensing of Dopamine Using Unmodified Gold Nanoparticles. *Sens. Actuators, B* **2011**, *156*, 95–99.
78. Mathews, T. A.; Fedele, D. E.; Coppelli, F. M.; Avila, A. M.; Murphy, D. L.; Andrews, A. M. Gene Dose-Dependent Alterations in Extraneuronal Serotonin but Not Dopamine in Mice with Reduced Serotonin Transporter Expression. *J. Neurosci. Methods* **2004**, *140*, 169–181.